Analysis of Stirling engine and comparison with other technologies using low temperature heat sources

Tamrat Abishu Gelu
Instituto Superior Técnico, Lisbon, Portugal

Abstract

In this study, the thermodynamic performance of two different low grade temperature heat conversion technologies: the Stirling engine and the Organic Rankine Cycle (ORC) are evaluated. The Stirling engine is studied using helium as a working gas for the conversion of low grade waste heat at 250^0C into electricity. The effects of regenerator effectiveness, hot temperature and phase angle are studied. Thermal efficiency of 20.2 % is attained. The ORC is integrated with a solar thermal system to provide 2 kW of electricity. Six different organic working fluids are studied. Energy and exergy analysis is performed for each component of the ORC. Among the fluids studied, R123 and n-Pentane showed higher performance and thermal efficiency.

Key words: Low grade heat, Stirling engine, Organic Rankine Cycle, energy and exergy analysis, thermodynamic model

1. Introduction

In recent years, the Stirling engine and the Organic Rankine Cycle (ORC) have become more attractive technology for energy conversion. Several researchers have showed interest in analyzing and developing the Stirling engine and the ORC for different applications. Sripakagorn et. al. [1], Tavakolpour et. al. [2] and Kongtragool et.al. [3, 4] studied conversion of solar energy in to electricity using the Stirling engine. Mehta et. al. [5] and Li et.al. [6] analyzed conversion of waste heat using the Stirling engine. Calise et.al [7], Pikra et. al. [8], Jing et. al. [9], Quoilin [10], Wolpert et.al. [11] showed the application of ORC for solar energy conversion. Hung et. al. [12], Wie et. al. [13] and Wang et. al. [14] studied the conversion of waste heat using ORC. Hettiarachchi et. al. [15], Shengjun et. al. [16] and DiPippo [17] investigated the application of ORC in geothermal heat conversion. These studies have showed the potential of these technologies for utilization of low grade temperature heat for electricity generation.

The Stirling engine in this study is used to generate electricity from waste heat at 250^0C, and the ORC is investigated for production of 2 kW from solar thermal system. Detailed thermodynamic cycle analyses for the two cycles are presented and their performances are evaluated. The first part presents the analysis of the Stirling engine while the ORC is studied in the second part of the report.

2. Stirling engine

Thermodynamic cycle analysis of alpha type Stirling engine configuration, Fig. 1, is studied in this section. Alpha type engines features two pistons, called hot and cold pistons, in two separate cylinders. The two pistons shuttle the working fluid from one cylinder to the other through a conduit which consists of a cooler, regenerator and heater arranged in series. The effects of hot space, cold space and regenerator dead volumes are taken into account in the analysis. The effect of varying the effectiveness of the regenerator, hot temperature and phase angle on the system performance is investigated.

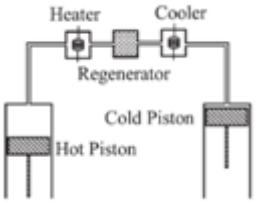

Fig. 1. Alpha type Stirling engine configuration [4].

2.1. Modeling

Isothermal model of the Stirling engine is considered in this study. It has two isothermal compression and expansion processes, and two isochoric processes, Fig. 2. Process 1–2 is an isothermal compression process; Process 2–3 is a constant volume regenerative transfer process; Process 3–4 is isothermal expansion process; and Process 4–1 is constant volume regenerative transfer process.

Fig. 2. The isothermal model of Stirling engine cycle.

2.2. Stirling engine thermodynamics analysis

The Stirling engine studied in this report is modeled based on the first order analysis (Schmidt analysis). The thermodynamics analysis of the cycle is performed in EES environment [18]. Results from the analysis are presented and discussed. It is assumed that the cycle is under steady state condition, the working gas obeys perfect gas law: $PV=mRT$, the mass of the working gas is constant and there is no leakage, volume variation in the working spaces is sinusoidal, the temperatures in the cold space, hot space and regenerator are isothermal at T_C, T_H and T_R respectively, pressure is constant in each space, the speed of the engine is constant.

The equations used for the analysis of the Stirling engine under the isothermal assumption and considering the dead volumes of the regenerator, hot and cold spaces are summarized below. Detailed analysis can be found in [19].

Total dead volume V_S is the sum of the hot, regenerator and cold space dead volumes, V_{SH}, V_{SR} and V_{SC} respectively:

$$V_S = V_{SH} + V_{SR} + V_{SC} = (k_{SH} + k_{SR} + k_{SC})V_S \qquad 1$$

Where: $k_{SH} = V_{SH}/V_S$, $k_{SR} = V_{SR}/V_S$, $k_{SC} = V_{SC}/V_S$ are the hot, regenerator and cold space dead volume ratios.

Regenerator effectiveness: $e = (T_{3'} - T_1)/(T_3 - T_1)$ 2

Regenerator effective temperature: $T_R = (T_{3'}+T_{1'})/2 = (T_3+T_1)/2$ 3

Total mass of the working fluid is the sum of masses contained in each space:

$$m = m_H + m_{SH} + m_R + m_C + m_{SC} \quad 4$$

Instantaneous system pressure: $p = mR / (V_H/T_3 + K + V_C/T_1)$ 5

where: $K = V_{SH}/T_3 + V_{SR}/T_R + V_{SC}/T_1$ 6

Mean pressure: $p_m=(mR/V_P)\{T_3 \ln[(V_D+V_P+KT_3)/(V_D+KT_3)]-T_1 \ln[(V_D+V_P+KT_1)/(V_D+KT_1)]\}$ 7

Total heat input: $Q_{in}=mC_V\{(1-e)(T_3-T_1)+(k-1)T_3 * \ln[(V_D+V_P+KT_3)/(V_D+KT_3)]$ 8

Where: k is the specific heat ratio

Total heat rejected: $Q_{in}= -mC_V\{(1-e)(T_3-T_1)+(k-1)T_1 * \ln[(V_D+V_P+KT_1)/(V_D+KT_1)]$ 9

Net work output: $W_{net}=mR\{T_3 \ln[(V_D+V_P+KT_3)/(V_D+KT_3)]-T_1 \ln[(V_D+V_P+KT_1)/(V_D+KT_1)]\}$ 10

Thermal efficieny: $\eta_{th}=W_{net}/Q_{in}$ 11

Carnot efficiency: $\eta_{carnot}=1 - T_1/T_3$ 12

2.3. Results and discussion

The performance of the Stirling engine is evaluated and the results are presented in this section. The input values used for the analysis are given in Table 1. Results of the analysis at the input values are also presented. The effect of varying the effectiveness of the regenerator, hot temperature and phase angle on the cycle efficiency, heat input and net work output are studied and the results are given in Figs. 3 to 5.

Table 1. Input values of the Stirling engine analysis.

Parameters	Unit	Value
Working gas		Helium
Hot temperature, T_H	K	523
Cold temperature, T_C	K	353
Regenerator effectiveness, e		0.894
Compression ratio, CR		1.5
Engine speed, n	Rpm	
Phase angle, ϕ	Degree	

2.3.1. Effect of regenerator effectiveness

The thermal efficiency and heat transfers at the cooler, heater and regenerator are dependent on the effectiveness of the regenerator. But, the regenerator effectiveness has no effect on the output work and the maximum power output [19, 20]. Regenerator with high effectiveness value improved the cycle efficiency and reduced the required heat input, Figs. 3(a) and (b), respectively. An increase in effectiveness from 0.8 to 0.9 increases the cycle efficiency from 18.3% to 20.1% and reduced the total

heat input from 0.96 kJ to 0.88 kJ. This is expected because the thermal efficiency is inversely related to the heat input; and a regenerator with high effectiveness value is capable of storing and releasing large amount of heat therefore reducing the required external heat input.

(a)

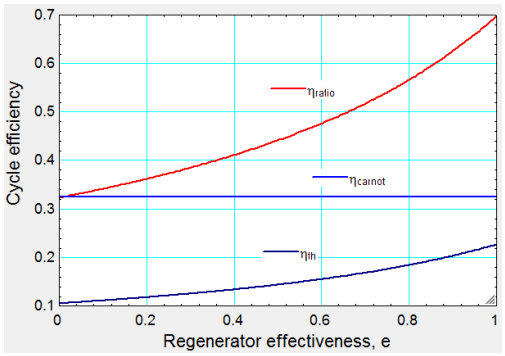

(b)

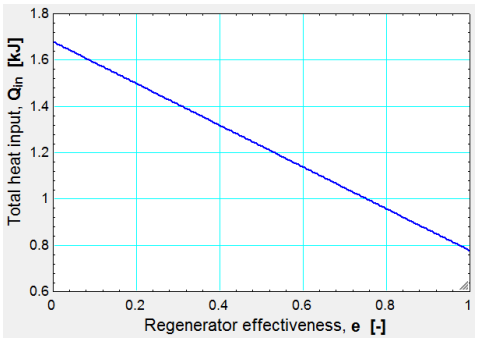

Fig. 3. Effect of regenerator effectiveness: (a) on cycle efficiency, (b) on total heat input.

2.3.2. Effect of hot temperature

Figs. 4(a) and (b) illustrate the effect of hot temperature on the cycle efficiency, total heat input and net work output. The efficiency, heat input and new work output of the cycle increased with increasing hot temperature. As can be seen in the theoretical T-S diagram of Stirling engine in Fig. 2, line 3-4 is in isothermal heat addition process and the area under this line is the heat input. Therefore, increasing the hot temperature increases the area under the isothermal heat addition line (process 3-4). The cold temperature was fixed at T_C=353K, therefore the area under process 1-2 has not changed during this process. The net work output is the difference of the areas under process 3-4 and process 1-2. Therefore, increasing the hot temperature increases the net work output (Fig. 4(b)).

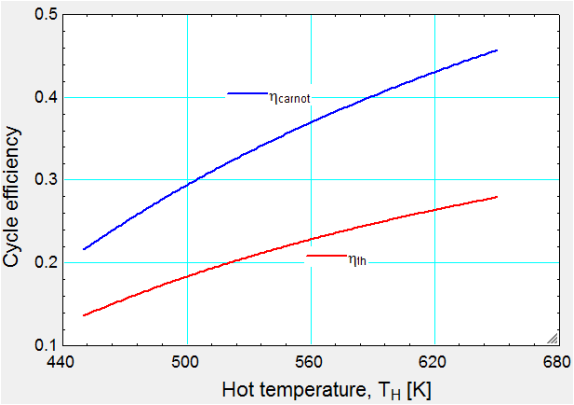

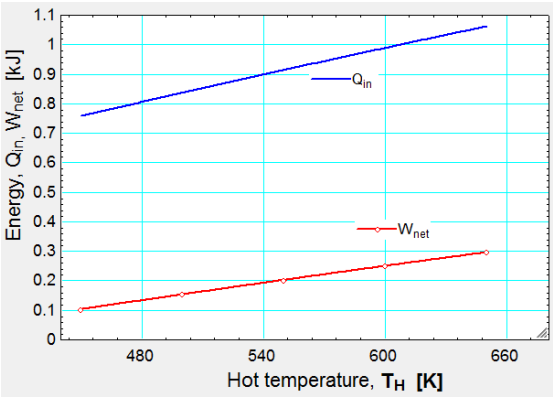

Fig. 4. Effect of hot temperature on: (a) cycle efficiency, (b) heat input and net work.

In general, increasing hot temperature increases the net work output and thermal efficiency of the engine but the highest temperature is limited by the induced thermal stress that the material can resist [35].

2.3.3. Effect of phase angle

Fig. 5(a) presents the effect of changing the phase angle between power and displacer pistons. It is observed that increasing the phase angle reduced both the heat input and net work output. But the cycle

efficiency did not change. Increasing the phase angle has a positive advantage in reducing the required heat input at the cost of reducing the net work output. Therefore, an optimal phase angle should be used in designing a Stirling engine. In the present study a phase angle of 90^0 is used. A phase angle of 90^0 is suggested as optimal [21] for a Stirling engine. Fig. 5(b) shows the P-V diagram of the Stirling cycle engine at phase angle of 90^0. This is way different from the theoretical Stirling cycle P-V diagram in Fig. 2, although does not correspond yet to the actual diagram.

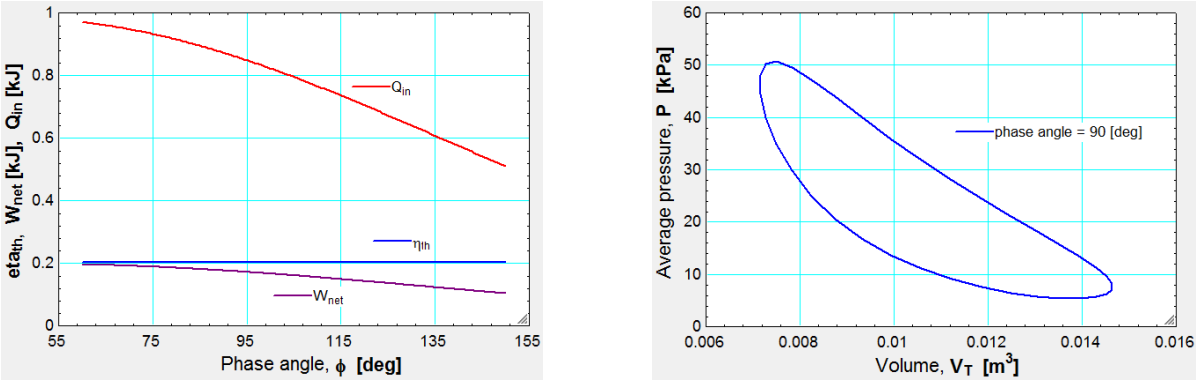

Fig. 5. (a) Effect of phase angle on performance of engine; (b) P-V diagram at 90^0 phase angle.

3. Solar ORC system modeling

The solar ORC system model in this study is adopted from [22], Fig. 6. The solar thermal system consists of 300 flat plate collectors with gross area of 600 m^2, a pump and a storage tank. It designed to provide hot water at 90^0C to the evaporator of the ORC system and, after passing through the preheater, it returns it at 76^0C. The ORC system consists of a condenser, pump, preheater, evaporator and expander. It is designed for a 2 kW power output, and is assumed to operate only during the day time for 8 hours when the solar radiation is high, i.e. from 9 am to 5 pm. Operation of the ORC at night or when there is low/no solar radiation requires a heat storage tank. But, significant amount of heat losses through the heat storage tank and pipes makes the solar ORC system unfeasible to be operated using stored heat for longer period. In addition, operating in part-load condition might reduce the performance of the ORC.

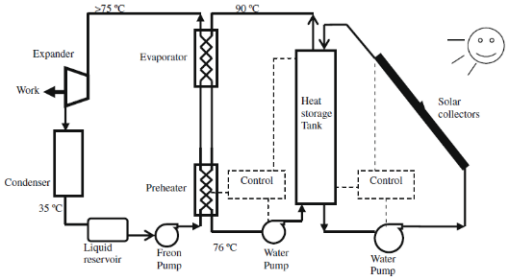

Fig. 6. Layout of solar powered ORC used in the present study, modeled by [22].

The cycle is modeled in EES environment [18]. Each of the state point thermodynamic properties is determined and the performance of the cycle is evaluated. The performance of the ORC is evaluated based on the first and second laws of thermodynamics for different organic working fluids. The properties of the selected organic working fluids are given in Table 2.

Table 2: Properties of organic fluids analyzed in this study

Fluid	Molecular Formula	Molecular mass (kg/kmol)	P_{crit} (MPa)	T_{crit} (K)	T_{bp} (K)	ATL (yr)	ODP	GWP (100yr)
R123[i]	$C_2HCl_2F_3$	152.93	3.67	456.85	300.95	1.3	0.012	77
R134a[i]	$C_2H_2F_4$	102.03	4.06	374.18	247.08	14	0	1430
R600a[i]	C_4H_{10}	58.12	6.64	407.85	261.41	0.019	0	~ 20
R245fa[d]	$C_3H_3F_5$	134.05	3.64	427.21	288.29	8.8	0	820
R600[d]	C_4H_{10}	58.12	3.80	425.15	272.63	0.018	0	~ 20
n-Pentane[d]	C_5H_{12}	72.15	3.39	460.35	300.95	0.01	0	~ 20

It is assumed that the system is under steady state condition, no pressure drops in connecting pipes and heat exchanger, the ambient temperature is 25 ^{0}C, the exit temperature of the heat source stream after the evaporator is equal to the inlet temperature to the preheater, heat losses in each component are ignored and working fluid entering the expander is saturated vapor.

The thermodynamic equations used to describe individual component performance and cycle efficiency are summarized below.

Pump**:** work input $\dot{W}_p = \dot{m}_{ORC}(h_5 - h_4)/\eta_p$ 13

exergy $\dot{I}_p = T_0\dot{m}_{ORC}(s_5 - s_4)$ 14

Preheater: heat added $\dot{Q}_{pre} = \dot{m}_{ORC}(h_6 - h_5)$ 15

exergy $\dot{I}_{pre} = T_0\dot{m}_{ORC}[(s_6 - s_5) - (h_6 - h_5)/T_{mid}]$ 16

T_{mid} is the midpoint temperature of the heat source between the evaporator and preheater which is determined by pinch point analysis.

Evaporator: heat added $\dot{Q}_e = \dot{m}_{ORC}(h_2 - h_1)$ 17

exergy $\dot{I}_e = T_0\dot{m}_{ORC}[(s_2 - s_1) - (h_2 - h_1)/T_H]$ 18

Expander: work output $\dot{W}_t = \dot{m}_{ORC}(h_3 - h_2) * \eta_p$ 19

exergy $\dot{I}_t = T_0\dot{m}_{ORC}(s_3 - s_2)$ 20

volume expansion ratio: $VER = \frac{v_3}{v_2}$ 21

Condenser: heat removed $\dot{Q}_c = \dot{m}_{ORC}(h_4 - h_3)$ 22

exergy $\dot{I}_c = T_0\dot{m}_{ORC}[(s_4 - s_3) - \frac{(h_4 - h_3)}{T_C}]$ 23

Total exergy destruction rate: $\dot{I}_{tot} = \dot{I}_p + \dot{I}_{pre} + \dot{I}_e + \dot{I}_t + \dot{I}_c$ 24

Total heat input: $\dot{Q}_{in} = \dot{Q}_e + \dot{Q}_{pre}$ 25

First law efficiency: $\eta_{ORC} = \frac{\dot{W}_{net,ORC}}{\dot{Q}_{in}}$ 26

Second law efficiency: $\eta_{II} = \frac{\eta_{ORC}}{1 - \frac{T_C}{T_H}}$ 27

3.1. Results and discussion

Thermodynamic cycle analysis of the solar powered ORC is performed using different organic working fluids under the same working condition. The working conditions (input values) of the ORC are given in

Table 3. Operating conditions of the solar powered ORC.

Evaporating temperature, T_e	75 ^{0}C
Condensing temperature, T_c	35 ^{0}C
Ambient temperature, T_0	25 ^{0}C
Turbine efficiency, η_t	0.441
Pump efficiency, η_p	0.8

Table 3. This input values are similar with the input value used in [22]. The properties of the organic working fluids considered in this study are also given in Table 2. The heat source temperature, i.e. the hot water coming from the solar thermal system, is 90^0 C and the temperature difference in the evaporator between the working fluid and heat source is set constant at 15^0 C. Results of the analysis at the operating condition are summarized in Table 4. Validity of the computation is verified by comparing part of the results obtained in this work with the wok of [22], Table 5. As it can be seen, good agreement in the thermal efficiency and mass flow rate of the working fluid was achieved.

Table 4. Performance comparison of different working fluid for T_e*=348K*, T_c*=308K* and *2kW* power output.

	$\dot{m}_{ORC}$ *(kg/s)*	η_{th} *(%)*	η_{II} *(%)*	$\dot{W}_p$ *(kW)*	Δh_{fg} *(kJ/kg)*	$\dot{I}_{total}$ *(kW)*	*VER*	$\dot{Q}_{in}$ *(kW)*	$\dot{m}_{source}$ *(kg/s)*	$\dot{V}_{source}$ *(lit/hr)*	$T_{mid,hot}$ *(K)*
R123[i]	0.234	4.460	24.91	0.0611	148.3	5.775	3.391	44.85	0.223	801.1	352.2
R134a[i]	0.302	3.711	20.72	0.475	116.1	7.253	3.876	53.9	0.496	1785	353.9
R245fa[i]	0.219	4.307	24.06	0.101	156.7	6.022	3.507	46.43	0.282	1014	352.7
R600[d]	0.117	4.241	23.68	0.150	300.6	6.152	2.961	47.16	0.279	1004	352.6
n-Pentane[d]	0.109	4.373	24.42	0.050	323.3	5.923	3.376	45.74	0.238	856	352.3
Isobutane[d]	0.134	4.075	22.76	0.231	261.1	6.461	2.885	49.08	0.338	1217	353.0

Table 5. Comparison of results of present work with Tchanche et al. work [22].

Fluid	Thermal efficiency		Mass flow rate	
	This work	[22]	This work	[22]
R123	4.460	4.457	0.2343	0.227
R134a	3.711	3.703	0.3018	0.244
R600	4.241	4.236	0.1166	0.108
R600a	4.075	4.055	0.1339	0.122

The effects of varying turbine inlet temperature on the system efficiency, exergy destruction rate, total heat input, working fluid mass flow rate and turbine exit volume flow rate are presented and discussed below.

3.1.1. ORC system efficiency

As shown in Table 4, for the considered operating condition, the first law thermal efficiency of the ORC varies from *3.71 %* for R134a to *4.46 %* for R123. The effect of varying the turbine inlet temperature on the first and second law efficiencies are shown in Figs 7(a) and (b) respectively. In all the cases there is no superheating and the fluids enter the turbine as saturated vapor.

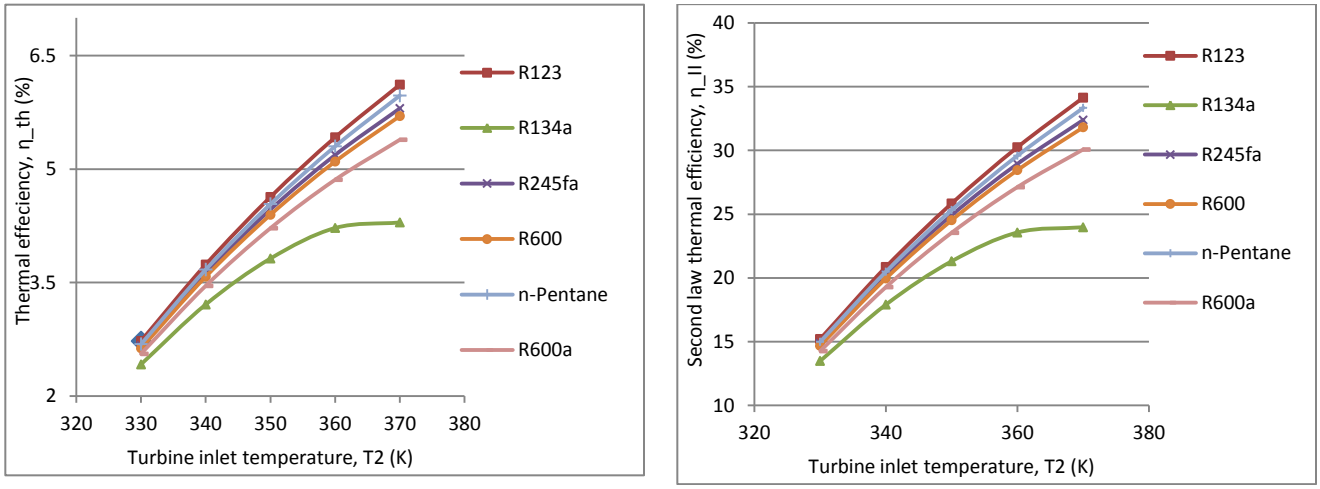

(a) (b)

Fig. 21. Effect of turbine inlet temperature on: (a) thermal efficiency, (b) the second law thermal efficiency, for different working fluids at $T_c=35^0C$ and $x_2=1$.

As shown in the graphs, increasing turbine inlet temperature increases the first and second law thermal efficiencies of the system for all working fluids. Looking at Table 2 and Fig. 7, fluids with higher boiling point, also critical temperature, show better efficiency at higher turbine inlet temperature. Similar observation was reported in [23], where they stated that thermal efficiencies are strong functions of the critical temperatures of the working fluids. For fluid R134a, increasing the turbine inlet temperature near its critical temperature has very low effect on the cycle thermal efficiency.

3.1.2. Total exergy destruction rate

System irreversibility (exergy destruction rate) as a function of turbine inlet temperature is presented in Fig. 8(a). All the fluids show reduction in exergy destruction rate as the turbine inlet temperature rises. The exergy destruction rates of R123, R600, R245fa and n-Pentane is very close to each other. Again, for R134a increasing the turbine inlet temperature near its critical temperature has very small effect on the exergy destruction rate.

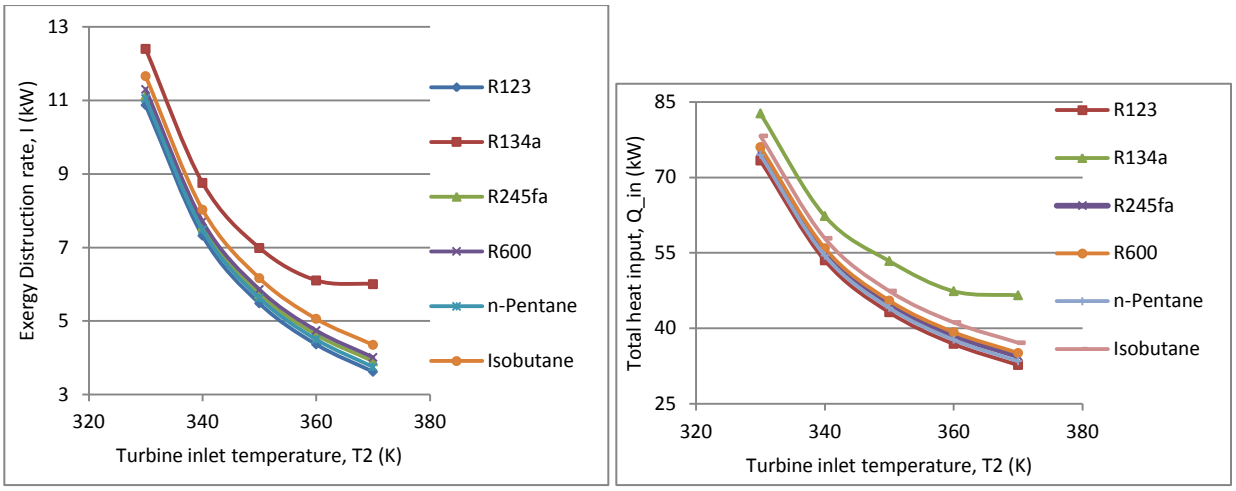

(a) (b)

Fig. 8. Effect of turbine inlet temperature on: (a) system exergy destruction rate, (b) total heat input, at $T_c=35^0C$ and $x_2=1$.

3.1.3. Heat input rate

Study of the heat input rate, Fig. 8(b), shows that each of the fluids requires less heat input at higher turbine inlet temperature. The heat input determines the size of the collector array, hence the cost of the system [22]. High heat input rate is required when the ORC is operated with R134a (53.9kW) and the lowest is when it is working with R123 (44.85 kW). n-Pentane, R245fa and R600 also have low heat input rates. Observing the heat source stream flow rate in Table 4, as the heat input increases the heat source stream flow rate also increases for the different fluids considered. Low heat source flow rate requires small size pump, heat storage tank and small number of solar collectors, therefore reduces the total cost of the system. Fluid R123 has the best advantage in this regard, followed by n-Pentane, R245fa, R600 and isobutane.

3.1.4. Mass flow rate

Fig. 9(a) shows the change in mass flow rate of the working fluid as a function of turbine inlet temperature. The mass flow rate of the working fluid depends on the enthalpy heat of vaporization Δh_{fg}[22]. Fluids with high enthalpy heat of vaporization require lower mass flow rate. This is observed in the present study, fluid R134a has the lowest heat of vaporization (*116.1 kJ/kg*) and highest mass flow rate (*0.302 kg/s*) while n-Pentane has the highest heat of vaporization (*323.3 kJ/kg*) and lowest mass flow rate (*0.109 kg/s*) in the range of temperatures considered and n-Pentane has the lowest.

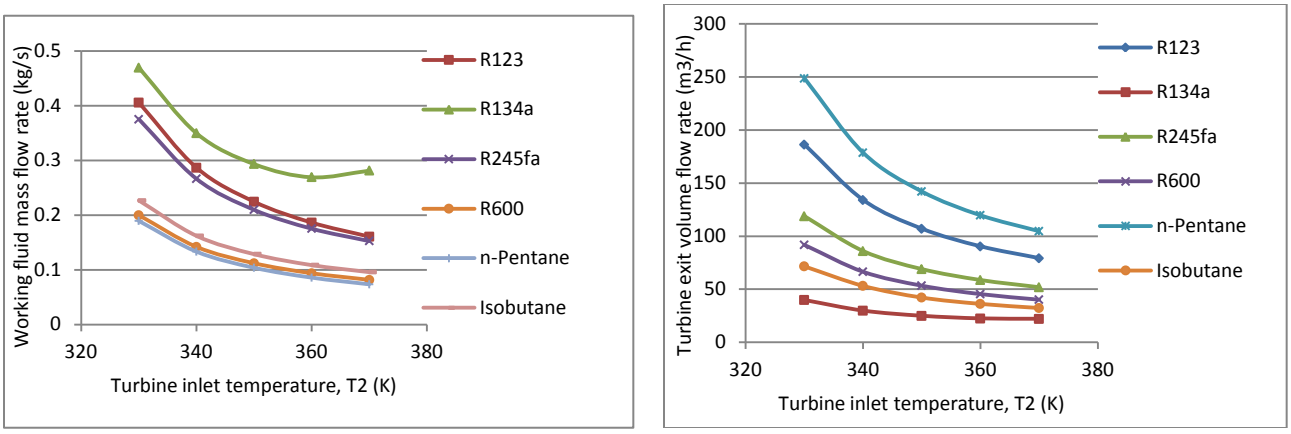

(a) (b)

Fig. 9. Effect of turbine inlet temperature on: (a) mass flow rate, (b) volume flow rate, $T_c=35^0C$ and $x_2=1$.

3.1.5. Volume flow rate

The volume flow rate of the fluid leaving the turbine determines the size, also cost, of the turbine. Fluids with higher specific volume ratio across the turbine will lower their effectiveness [22, 10]. As shown in Fig. 9(b), R134a has the lowest turbine exit flow rate and n-Pentane has the highest. Considering this, R134a has a better economical advantage, as it requires small size components [22].

4. Conclusion

This report presented two technologies for conversion of low grade heat: the Stirling engine and the organic Rankine cycle. Based on the study conducted on both systems the following conclusions can be made.

For Stirling engine:

- ✓ Increasing the hot side temperature increases the thermal efficiency, the total heat input and the net work output significantly.
- ✓ A Stirling engine with higher regenerator effectiveness value reduces the total heat input, hence increases the thermal efficiency.
- ✓ Increased dead volumes and low regenerator effectiveness has a negative impact on thermal efficiency.
- ✓ Higher phase angle between the hot and cold piston reduces the total heat input and the net work output.

For ORC:

- ✓ For all the fluids tested, increasing the evaporator temperature has economic as well as thermodynamic advantages. High evaporator temperature decreases the exergy destruction rate, the required heat input and the working gas mass flow rate. As a result of these, the first and second law thermal efficiencies increase. It also lowers the volume flow rate at the exit of the turbine, which in turn requires a small size turbine, and, therefore lowers the overall cost.

- ✓ Increasing the evaporator pressure has a negative effect on the ORC performance. It increases the heat input and the exergy destruction rate and as a result the thermal efficiency decreases for all the fluids.
- ✓ Increasing evaporator pressure also increases the volume flow rate at the expander exit and the working gas mass flow rate.
- ✓ Among the different fluids tested R123 has the highest efficiency and lowest heat input and exergy destruction rate followed by n-Pentane, R245fa, R600, isobutane and R134a. But fluid R134a has the lowest turbine exit volume flow rate followed by isobutane and R600. Therefore, the selection of ORC fluid is a tradeoff between cost and performance.

In general, in terms of their thermodynamics performance both technologies are feasible for conversion of low grade heat in to power (electricity). The choice between the two technologies lies on the temperature of available low grade heat and the required power output.

References

[1]. Sripakagorn A, Srikam C. Design and performance of a moderate temperature difference Stirling engine. Renewable Energy Vol. 36, pp. 1728-1733, 2011.

[2]. Tavakolpour AR, Zomorodian A, Golneshan AA. Simulation, construction and testing of a two-cylinder solar Stirling engine powered by a flat plate solar collector without regenerator. Renewable Energy Vol. 33, pp. 77-87, 2008.

[3]. A four power-piston low-temperature deferential Stirling engine using simulated solar energy as a heat source. Solar Energy Vol. 82, pp. 3493-500, 2008.

[4]. Kongtragool B, Wongwises S. A review of solar-powered Stirling engines and low temperature differential Stirling engines. Renewable and Sustainable Energy Reviews, Vol. 7, pp. 131-154, 2003.

[5]. Mehta AV, Gohil RK, Bavarva JP, Saradava BJ. Waste heat recovery using Stirling engine. International Journal of Advanced Engineering Technology Vol. 3, pp. 305-310, 2012.

[6]. Li T, Tang D, Li Z, Du J, Zhou T, Jia Y. Development and test of a Stirling engine driven by waste gases for the micro-CHP system. Applied Thermal Engineering Vol. 33-34, pp. 119-123, 2012.

[7]. Calise F, Capuozzo C, Vanoli L. Design and parametric optimization of an organic Rankine cycle powered by solar energy. American Journal of Engineering and Applied Sciences, Vol. 6, pp. 178-204, 2013.

[8]. Pikra K, Salim A, Prawara B, Purwanto AJ, Admono T, Eddy Z. Development of small scale concentrated solar power plant using organic Rankine cycle for isolated region in Indonesia. Energy Procedia Vol. 32, pp. 122-128, 2013.

[9]. Jing L, Gang P, Jie J. Optimization of low temperature solar thermal electric generation with organic Rankine cycle in different areas. Applied Energy Vol. 87, pp. 3355-3365, 2010.

[10]. Quoilin S, Orosz M, Hemond H, Lemort V. Performance and design optimization of a low-cost solar organic Rankine cycle for remote power generation. Solar Energy Vol. 85, pp. 955-966, 2011.

[11]. Wolpert JL, Riffat SB. Solar-powered Rankine system for domestic applications. Applied Thermal Engineering Vol. 16, pp. 281-289.

[12]. Hung TC, Shai TY, Wang SK. A review of Organic Rankine Cycles (ORC) for the recovery of low-grade waste heat. Energy Vol. 22, No. 7, pp. 661-667, 1997.

[13]. Wie G, Yiwu W, Guangyi C. Testing and thermodynamic analysis of low-grade heat poer generation system using organic Rankine cycle. International Conference on Power Engineering, October 23-27, 2007, Hangzhou, China.

[14]. Qiu G. Selection of working fluids for micro-CHP systems with ORC. Renewable Energy Vol. 48, pp. 565-570, 2012.

[15]. Hettiarachchi HDM, Golubovic M, Worek WM, Ikegami Y. Optimum design criteria for an Organic Rankine cycle using low-temperature geothermal heat sources. Energy Vol. 32, pp. 1698-1706, 2007.

[16]. Shengjun Z, Huaixin W, Tao G. Performance comparison and parametric optimization of subcritical organic Rankine cycle (ORC) and transcritical power cycle system for low temperature geothermal power generation. Applied Energy Vol. 88, pp. 2740-2754, 2011.

[17]. Sripakagom A, Srikam C. Design and performance of a moderate temperature difference Stirling engine. Renewable Energy, Vol. 36, pp. 1728-1733, 2011.

[18]. Klein SA. Engineering Equation Solver, F-Chart Software, 2010, Middleton, WI.

[19]. Wongwises S, Kongtragool B. Thermodynamic analysis of a Stirling engine including dead volumes of hot space, cold space and regenerator. Renewable Energy, Vol. 31, pp. 345-359, 2006.

[20]. Finite time thermodynamic evaluation of endoreversible Stirling heat engine at maximum power conditions. Renewable and Sustainable Energy Reviews, Vol. 16, pp. 2234-2241, 2012.

[21]. Thombare DG, Verma SK. Technological development in the Stirling cycle engine. Renewable and Sustainable Energy Reviews, Vol. 12, pp. 1-38, 2008.

[22]. Tchanche BF, Papadakis G, Lambrinos G, Frangoudakis A. Fluid selection for a low-temperature solar organic Rankine cycle. Applied Thermal Engineering Vol. 29, pp.2468-2476, 2009.

[23]. Aljundi I H. Effect of dry hydrocarbons and critical point temperature on the efficiencies of organic Rankine cycle. Renewable Energy Vol. 36, pp. 1196-1202, 2011.